INVESTIGATIONS OF STRUCTURAL AND OPTICAL PROPERTIES ON $Pr_{0.7}Sr_{0.3}MnO_3$/ $Gd_{0.7}Sr_{0.3}MnO_3$/ $Dy_{0.7}Sr_{0.3}MnO_3$

A dissertation submitted to
INDIAN INSTITUTE OF TECHNOLGY HYDERABAD
in partial fulfillment for the award of degree of

Master of Science
By
Soumita Mondal
PH13M1014

Under the supervision of
Dr Saket Asthana
DEPARTMENT OF PHYSICS

भारतीय प्रौद्योगिकी संस्थान हैदराबाद
Indian Institute of Technology Hyderabad

INDIAN INSTITUTE OD TECHNOLOGY HYDERABAD
INDIA

APRIL 2015

Declaration

I declare that this written submission represents my ideas in my own words, and where others' ideas or words have been included, I have adequately cited and referenced the original sources. I also declare that I have adhered to all principles of academic honesty and integrity and have not misrepresented or fabricated or falsified any idea/data/fact/source in my submission. I understand that any violation of the above will be a cause for disciplinary action by the Institute and can also evoke penal action from the sources that have thus not been properly cited, or from whom proper permission has not been taken when needed.

Soumita Mondal.

(Signature)

__SOUMITA MONDAL__

(– Student Name –)

____PH13M1014_

(Roll No)

Approval Sheet

This thesis titled "**INVESTIGATIONS OF STRUCTURAL AND OPTICAL PROPERTIES ON $Pr_{0.7}Sr_{0.3}MnO_3$/ $Gd_{0.7}Sr_{0.3}MnO_3$/ $Dy_{0.7}Sr_{0.3}MnO_3$** " by SOUMITA MONDAL is approved for the degree of Master of Science from IIT Hyderabad.

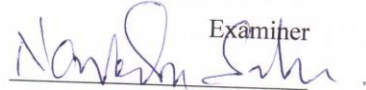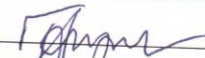-Dr Prem Pal-

Co-ordinator/Examiner

05/05/15

-Dr Vandana Sharma-

Examiner

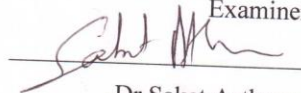-Dr Narendra Sahu-

Examiner

-Dr J.Suryanarayan-

Examiner

-Dr J. Mohanty-

Examiner

-Dr S.Hundi-

Examiner

-Dr Saket Asthana-

Adviser

DEDICATED TO MY PARENTS AND BROTHER

ACKNOWLEDGEMENTS

First and foremost, I would like to express my sincere gratitude to my advisor, Dr. Saket Asthana for the continuous support of my project work, for his patience, motivation, enthusiasm, immense knowledge and constructive criticism. His guidance has helped me al throughout my project and writing of this thesis.
I could not have imagined having a better advisor and mentor for my project study.

I am extremely grateful to The Head of Department, Dr. Anjan Kumar Giri, for providing excellent laboratory facilities and nice atmosphere for doing my project. Also, I would like to extend my sincere regards to all the nonteaching staff of Department of Physics for their support during the lab sessions.

During this time, I have learned a lot from Mr V.Sudarshan who is under my supervisor. He took keen interest in my project and guided me all along, till the completion of my project work. I am thankful to him with my humble acknowledgement for his constant encouragement and support from the beginning till the successful completion of the project.

Finally I would like to express my sincere gratitude to my parents for their constant support and encouragement.

ABSTRACT

In this project titled "**INVESTIGATIONS OF STRUCTURAL AND OPTICAL PROPERTIES ON $Pr_{0.7}Sr_{0.3}MnO_3$/ $Gd_{0.7}Sr_{0.3}MnO_3$/ $Dy_{0.7}Sr_{0.3}MnO_3$** " I have studied the structural and optical properties of the three compounds. The very basic theoretical knowledge has been described in the beginning that is required for the understanding of the structural and optical properties. The reason for the distortion and anomalous behavior of this class of compounds has been well dealt in the theoretical part. Then the step by step procedure of the preparation of the compounds by solid synthesis route has been explained along with a flow chart for a better understanding. The compounds have been prepared by solid state reaction procedure. All the samples have crystallized in Pnma space group. With the help of XRD pattern analysis Miller indices, particle size, strain and lattice parameters have been found out. SEM images have been used to explain the morphology and the grain size. Further FTIR and RAMAN spectroscopy has been used to study the optical properties, modes of vibrations and the MnO_6 octahedral structure.

CONTENTS

List of figures

List of tables

Chapter 1

INTRODUCTION

Alkaline rare earth doped manganites are perovskite type oxides (ABO_3), with rare earth element and Strontium in the A-site and Manganese as a transition metal in the B-site. They have been widely studied mainly due to their interesting catalytic oxygen cathode reduction and mixed electronic–ionic conduction properties[1-4]. Most of these applications are related to the LANTHANUM STRONTIUM MANGANITES (LSMO) ability to perform the adsorption and reduction of molecular oxygen, and the subsequent transport of the oxide ions formed[5-15]. The partial substitution of the lanthanum in $LaMnO_3$ by aliovalent cations, like Sr^{2+}, promotes morphological, chemical and crystallographic changes. The Mn-O bond length and Mn-O-Mn bond angle, the oxygen distribution, the number of cation vacancies and Mn^{3+}/Mn^{4+} concentrations are strongly affected by the Sr content[16-19]. The electric transport and magnetic properties of these manganites are closely related to the Mn oxidation state, which is determined by the oxygen content of the sample. Many authors suggest that the Mn^{3+}/Mn^{4+} ratio is a unique parameter for understanding the colossal magnetoresistance effect as well as the transition from the ferromagnetic metal to the paramagnetic. The metal insulator transition is very simply observable as a resistance peak in the $\rho(T)$ dependence and T_{MI} corresponds to the temperature of the maximal resistance.

The compounds that I have studied is $R_{0.7}Sr_{0.3}MnO_3$, where R is Dysprosium (Dy), Gadolinium (Gd) and Praseodymium (Pr).

Objectives behind choosing this family of compounds

Alkaline earth doped perovskite manganites have been a focus of research during the past several years on account of the following few interesting phenomena and their applications:
Magnetocaloric effect (MCE) provides a unique way of realizing the refrigeration from ultra-low temperature to room temperature. With the increase of applied field, magnetic entropies decrease and heat is radiated from the magnetic system into the environment through an isothermal process, while with the decrease of applied field, magnetic entropies increase and heat is absorbed from the lattice system into the magnetic system through an adiabatic process. Both the large isothermal entropy change and the adiabatic temperature change characterize the prominent MCE. **Magneto-resistance** and its application in magnetic information storage technology and could be the key to the next generation of magnetic memory devices or magnetic-field sensors. Electrical conductivity increases with an increase in the amount of Sr content. Mn^{3+}/Mn^{4+} is a unique parameter. On account of charge balancing by the doping of Sr^{2+}, conversion of Mn^{3+} to Mn^{4+} takes place. Mn^{4+} occurs in the ratio of Sr^{2+}. The substitution of group 2 i.e. Sr^{2+} in $RMnO_3$ produces acceptors. The substitution of R^{3+} ions for Sr^{2+} in $SrMnO_3$ creates donors. The manganites with x<0.5 in $R_{1-x}Sr_xMnO_3$ are hole doped. I have made the study using x=0.3. The **steep drop in resistivity with temperature** accompanying an insulator-metal transition is the phenomenon relevant to the bolometric application.

The present thesis is organized as follows:
Chapter 2 describes the theoretical background, Chapter 3 explains the experimental details, Chapter 4 presents the results and discussions and finally chapter 5 gives the conclusions and future work.

Chapter 2

THEORETICAL BACKGROUND

The study of this class of compounds needs a good theoretical knowledge on a few topics. Before we proceed towards experimental details and results we need to have a basic understanding on the structure of the compound and the mechanisms which give these compounds very peculiar and rare characteristics that have been used for many purposes in the modern society.

2.1 BRIEF STUDY OF PEROVSKITE STRUCTURE

The mineral perovskite (CaTiO3) is named after a Russian mineralogist, Count Lev Aleksevich von Perovski, and was discovered and named by Gustav Rose in 1839 from samples found in the Ural Mountains. Since then considerable attention has been paid to the perovskite family of compositions. The perovskite is a true engineering ceramic material with a plethora of applications spanning energy production (SOFC technology), environmental containment (radioactive waste encapsulation) and communications (dielectric resonator materials)

Crystallography of The Perovskite Structure

The perovskite structure has the general stoichiometry ABX_3, where "A" and "B" are cations and "X" is an anion. The "A" and "B" cations can have a variety of charges and in the original Perovskite mineral ($CaTiO_3$) the A cation is divalent and the B cation is tetravalent. However, for the purpose of this study, the case where A cations were restricted to being rare earth strontium $R_{1-x}Sr_x$ (where R is Dy, Gd, Pr), B is Manganese (Mn) and X is Oxygen (O). Due to the large number of perovskite compositions possible from combinations of cations on the lattice site, 96 compositions were chosen. The traditional view of the perovskite lattice is that it consists of small B cations within oxygen octahedra, and larger A cations which are XII fold coordinated by oxygen. This structural family is named after the mineral CaTiO3 which exhibits an orthorhombic structure with space group Pnma [100,101].
The structure of an ideal cubic perovskite is shown in Figure 2.1, where the A cations are shown at the corners of the cube, and the B cation in the centre with oxygen ions in the face-centred positions. The spacegroup for cubic perovskites is Pm3m (221) [102] .The equivalent positions of the atoms are detailed in Table 2.1.
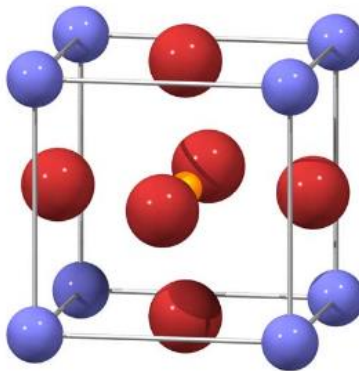

Fig 2.1 –Perovskite Structure

TABLE 2.1 THE POSITIONS OF THE IONS

SITE	CO-ORDINATES
A cation	(0,0,0)
B cation	(½, ½, ½)
O anion	(½, ½, 0), (½, 0, ½), (0, ½, ½)

2.2 ELECTRONIC STRUCTURE AND DOPING: QUALITATIVE PICTURE

$R_{1-x}Sr_xMnO_3$, shows interesting properties such as colossal magnetoresistance or charge-ordering [20] [21]. In this family, the replacement of R for divalent Sr^{2+} cations oxidizes Mn^{3+} to Mn^{4+}, introducing holes in the Mn 3d band and giving rise to metallic and/ or ferromagnetic behavior The presence of Mn^{3+} and Mn^{4+}, mixed valences gives rise to a double-exchange mechanism similar to that observed in A-substituted perovskites, increasing drastically the electrical conductivity and inducing ferromagnetic-like behavior with reentrant spin-glass character [22] [23].
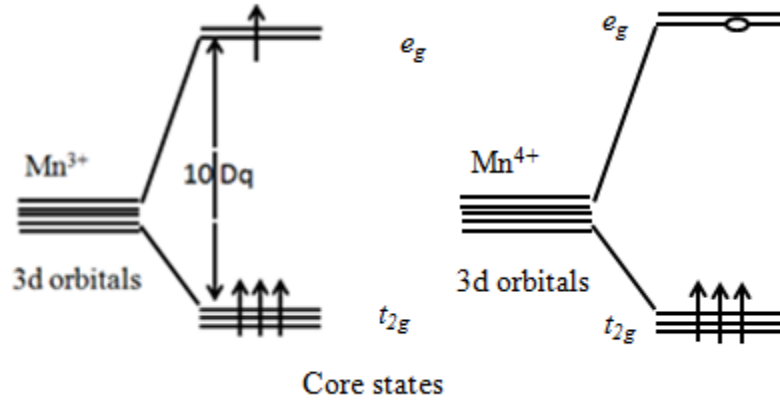

Fig 2.2 – Electronic Structure Of Mn^{3+} and Mn^{4+}

2.3 DOUBLE EXCHANGE HOPPING MECHANISM

The **double-exchange mechanism** is a type of a magnetic exchange that may arise between ions in different oxidation states. First proposed by Clarence Zener, this theory that predicts the relative ease with which an electron may be exchanged between two species, and has important implications for whether materials are ferromagnetic, antiferromagnetic, or neither. For example, consider the 180 degree interaction of Mn-O-Mn in which the Mn "e_g" orbitals are directly interacting with the O "2p" orbitals, and one of the Mn ions has more electrons than the other. In the ground state, electrons on each Mn ion are aligned according to the Hund's rule.

If O gives up its spin-up electron to Mn $^{4+}$, its vacant orbital can then be filled by an electron from Mn^{3+}. At the end of the process, an electron has moved between the neighboring metal ions, retaining its spin. The double-exchange predicts that this electron movement from one species to another will be facilitated more easily if the electrons do not have to change spin direction in order to conform with Hund's rules when going to the accepting species. The ability to hop (to delocalize) reduces the kinetic energy. Hence the overall energy saving can lead to ferromagnetic

alignment of neighboring ions. One of the manganese atoms has one of its e_g states occupied, the other has an empty e_g shell. One electron tunnels from the oxygen atom to the manganese atom without e_g electrons. The e_g electron from the other manganese atom, then tunnels to the free 2p position of the oxygen atom. The net result is one electron moving from one manganese atom to the next. This is how double exchange interaction induces electrical conductivity. Since electrons retain their spin while tunneling, tunneling is only possible between states with parallel spins. This is why double exchange interaction only occurs between manganese atoms whose t_{2g} electrons have their spins aligned. Because double exchange interaction increases the freedom of electrons, it lowers their energy. This makes it energetically favorable for electrons of neighboring manganese atoms to align their spins, inducing ferromagnetism. Since double exchange interaction requires filled e_g states as well as empty ones (holes) it is highly doping dependent. In double-exchange, the interaction occurs only when one atom has an extra electron compared to the other.[24] [25]
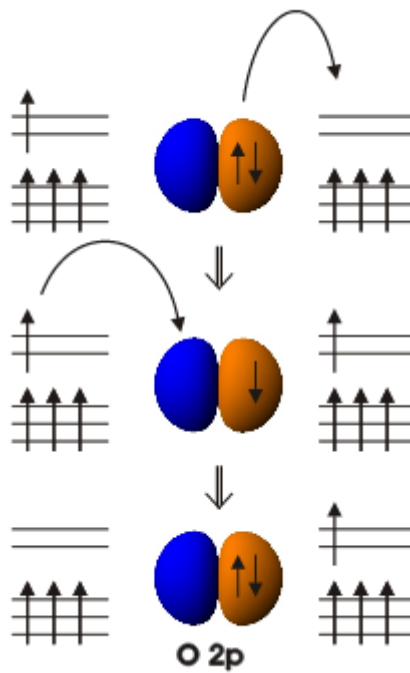

Fig 2.3 – Double exchange Interaction

2.4 SUPER EXCHANGE INTERACTION

Super exchange interaction occurs due to the slightly overlapping t2g and e_g orbitals of two neighboring manganese atoms. Electrons in the these shells can tunnel to the neighboring manganese atom. When this neighboring shell is already half filled, tunneling is only possible to the antiparallel spin states. Due to the Hund's interaction energy, these antiparallel states have a higher energy level, making the electrons tunnel back directly to their original manganese atom. However this tunneling possibility increases the freedom of the electrons, decreasing their energy. Since electrons retain their spin while tunneling, super exchange interaction is only possible between manganese atoms whose electrons have antiparallel spins. This makes it energetically favorable for electrons of neighboring manganese atoms to assume antiparallel spins. This induces antiferromagnetism.

2.5 JAHN- TELLER EFFECT

The Jahn Teller effect is an interaction effect between the crystal lattice and the manganese 3d electrons. Deformation of the oxygen octahedron causes energy differences within the otherwise degenerate t_{2g} and e_g electron states. This is shown in Fig 2.4. Orbitals which are compressed by the deformation, gain energy while orbitals which are elongated by the deformation lose energy. When the e_g shell is half filled it is energetically favorable to create a deformation, because one of the orbitals will lose energy. The electrons in the e_g shell will then occupy this lower energy state. Creating a deformation of the oxygen octahedrons without altering the overall crystal lattice leads to the typical Jahn Teller distortions shown in Fig 2.5. The Jahn Teller distortions are only favorable when a lot of manganese atoms have a half filled e_g shell. This makes this effect doping dependent. The degeneracy within the t_{2g} and e_g states can also be lifted by deformations due to externally imposed strain.
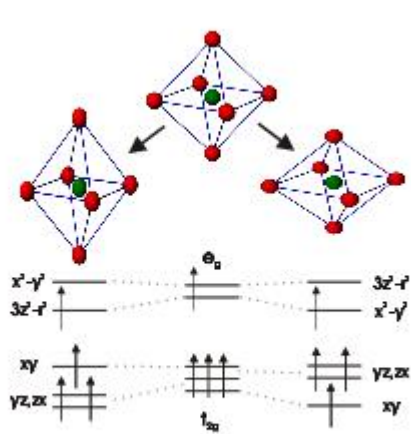

Fig 2.4- Jahn Teller Effect: Deformation of the Oxygen Octahedra lifts the degeneracy of the e_g and the t_{2g} level
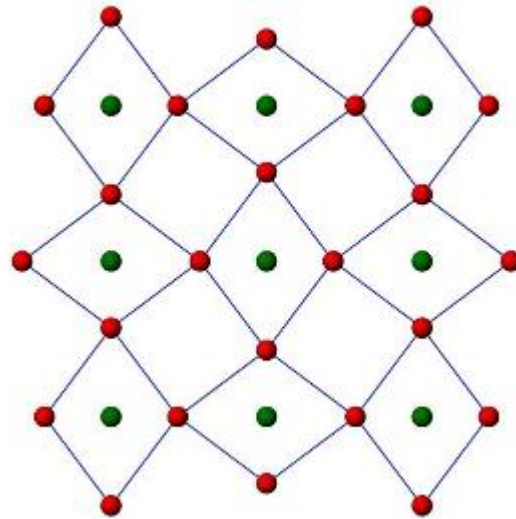

Fig 2.5- Lattice distortion due to Jahn Teller Effect. The Manganese atoms retain their positions while the oxygen octahedrons are deformed.

13

2.6 CHARGE ORDERING

Charge ordering is caused by Coulomb repulsion between e_g electrons at different manganese atoms. The electrons order themselves in a pattern shown in Fig 2.6. This configuration is so stable that electrons retain their positions preventing electrical conduction. This stability has two causes. The first one is the aforementioned Coulomb repulsion. The second one is electron phonon coupling. The electrons locally deform the oxygen octahedrons. To break the electron configuration the lattice would have to be reformed as well. Electrical ordering is only favorable for certain electron hole ratios, making it doping dependent.
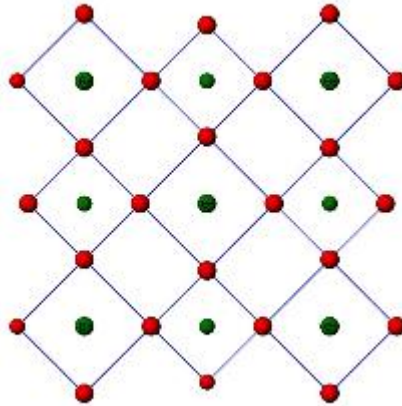

Fig- 2.6. Charge ordering for doping of x=0.5, e_g electrons spread over the manganese atoms due to coulomb repulsion. Due to this electron distribution the lattice gets deformed.

2.7 PHASE DIAGRAM

The four described mechanisms all contribute to the electric and magnetic properties of Rare Earth Doped Strontium Manganites. The temperature, doping, strain and shape of the sample determine which mechanism is dominant. This is clearly visible in a phase diagram as shown in Fig 2.7.
The abbreviations used in the phase diagram have their own distinctive meanings:
FM= Ferromagnetic, AF= Antiferromagnetic, CAF= Canted AF, FI= FM Insulator,
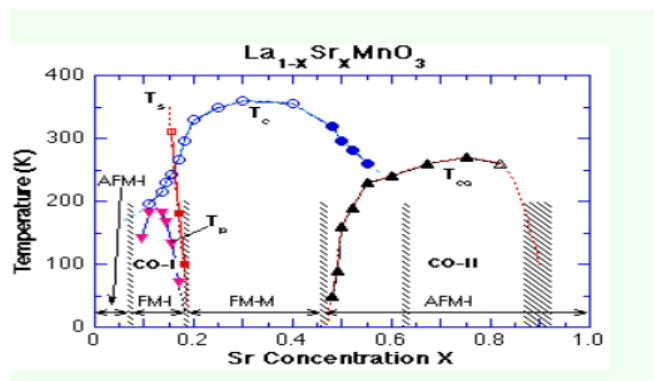CO= Charge Ordered
Maximum Magnet Resistance R at x=0.25-0.3

Fig 2.7 - Phase diagram of LSMO

14

2.8 TOLERANCE FACTOR

In an idealized cubic perovskite constructed of rigid spheres, each cation is the perfect size to be in contact with an oxygen anion, the radii of the ions can then be related:

$<R_A> + <R_o> = \sqrt{2}\,(<R_B> + <R_O>)$, where $<R_A>$, $<R_B>$ and $<R_O>$ are the average ionic radii of the A site and B site cations and the oxygen ion respectively. However with decreasing A cation size, a point will be reached where the cations will be small to remain in contact with the anions in the cubic structure.

Therefore, the B-O-B links bend slightly, tilting the BO_6 octahedra to bring some anions into contact with A cations. To allow for this distortion, a constant 't', is introduced into the above equation, thus :

$<R_A> + <R_o> = \sqrt{2}\, t(<R_B> + <R_O>)$, where 't' is the tolerance factor and can be used as a measure of the degree of distortion of a perovskite from ideal cubic. Therefore, the closer to cubic, the closer the value of tolerance factor is to unity. As $<R_A>$ or 't' decreases (0.96<t<1) the lattice structure can be transformed into rhombohedral and then into orthorhombic structure (t<0.96) where B-O-B bond angle is bent and deviated from 180 degrees.

Table 2.2 Calculation of Tolerance Factor

Compound Name	$<R_A>=0.7*R_{Rare}+0.3*R_{Sr}$ Rare= Dy^{3+}, Gd^{3+}, Pr^{3+}	$<R_B>$= radius of Mn^{3+}	$<R_O>$= radius of Oxygen	$t=\dfrac{<RA> + <Ro>}{\sqrt{2}\,(<RB> + <RO>)}$
$Dy_{0.7}Sr_{0.3}MnO_3$	0.7*1.24+0.3*1.44	0.645	1.4	0.934
$Gd_{0.7}Sr_{0.3}MnO_3$	0.7*1.27+0.3*1.44	0.645	1.4	0.941
$Pr_{0.7}Sr_{0.3}MnO_3$	0.7*1.32+0.3*1.44	0.645	1.4	0.953

From this calculation it is quite evident that the tolerance factor t<0.96, so the structure of the compounds studied is orthorhombic.

CHAPTER 3

EXPERIMENTAL DETAILS

3.1 Method Of Preparation

The polycrystalline samples of $R_{0.7}Sr_{0.3}MnO_3$ (R= Dy, Gd, Pr) have been synthesized by the solid state reaction route using the ingredients R_2O_3, $SrCO_3$ and Mn_2O_3. Each compound has been prepared 1 gram of mass. The ingredients had been mixed in proper stoichiometric ratio to obtain 1gram of the compound.

The calculation for obtaining 1 gram of $Pr_{0.7}Sr_{0.3}MnO_3$ has been shown below. We can proceed in the similar method for the other compounds too:

Here we calculate the mass of individual compound required to prepare 3 grams of the required compound:

$\frac{0.7}{2}(Pr_2O_3)+0.3(SrCO_3)+\frac{1}{2}(Mn_2O_3)$

$= 0.35\,(329.81) + 0.3(147.63) + 0.5(157.87)$

$= 115.4335 + 44.289 + 78.935$

$= 238.6575$

Now we calculate the mass of each of the individual compounds require for the preparation of 1 gram of the required compound:
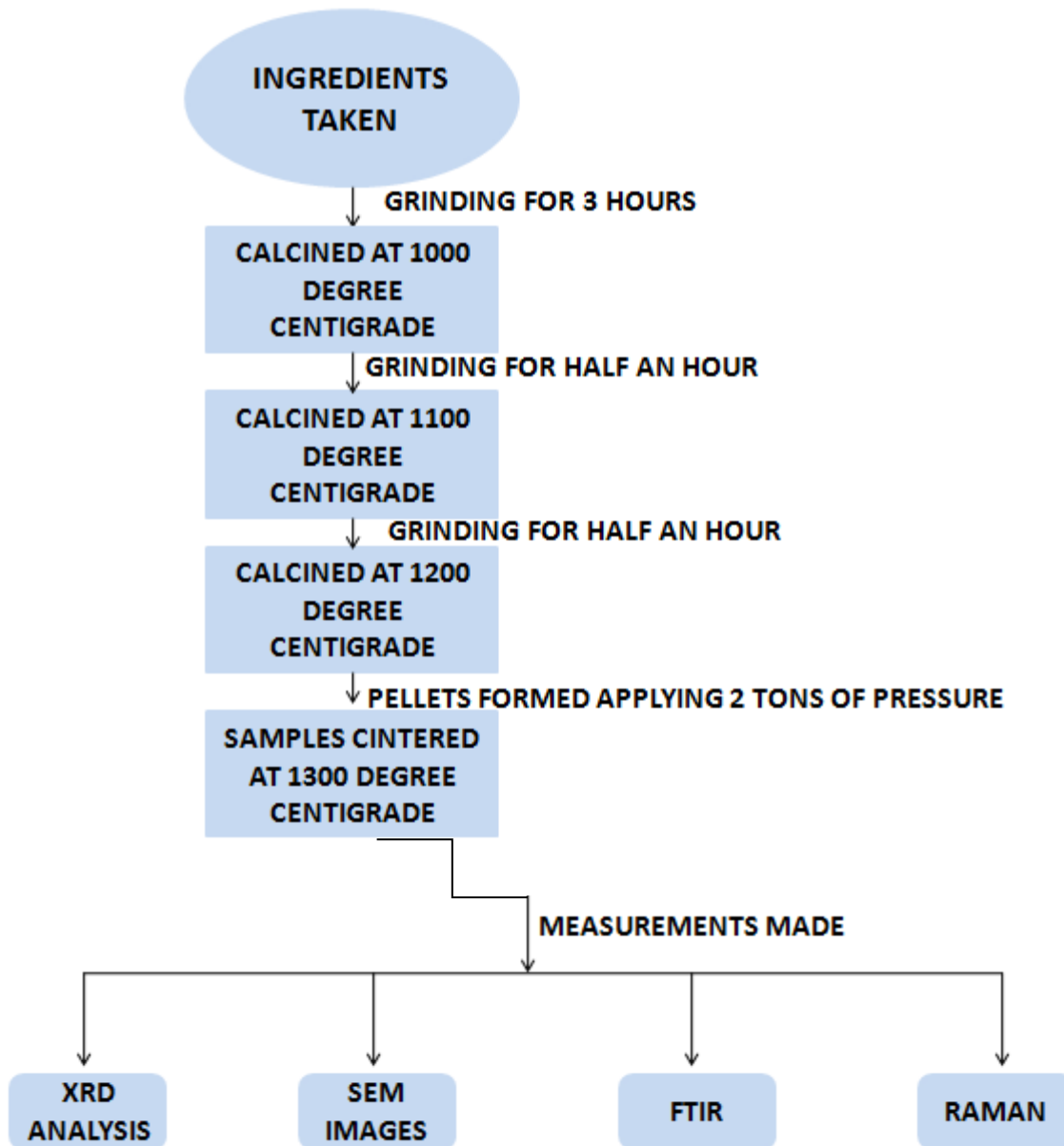
Pr_2O_3= 115.4335/238.6575= 0.483678

$SrCO_3$= 44.289/238.6575= 0.185576

Mn_2O_3= 78.935/238.6575= 0.330746

3.2 Steps Involved

- The individual ingredients were taken in a mortar pestel in proper stoichiometric ratio and grinded for three hours.

- Then the powder was calcined in air at 1000^0C, 1100^0C and 1200^0C for 12 hours each.

- After being calcined at a certain temperature intermediate grindin was done for half an hour again.

- Thereafter the calcined samples were pressed into pellets applying 2tons of pressure.

- The pellets were then sintered at 1300^0C for 12hours.

- The structure and phase purity of the samples were analyzed by powder X-Ray Diffraction (XRD) using CuK_α radiation (0.15406 nm). Form the XRD measurements I have determined the Miller Indices by comparing it with the JCPDS database and thus calculated particle size, strain and lattice parameters.

- Then I have obtained SEM images from where I could make a study of the Granular structure, porosity and grain boundaries of the samples. I have also calculated the grain size distribution using the images.

- FTIR (Fourier Transform Infrared Spectroscopy) was taken to study the fingerprint region of the compounds that is within the wave number <1000 cm^{-1}. A spectrum of characteristic bands is produced that can be used as a finger print to help identify and characterize the sample. FTIR analysis can be conducted in transmission or reflection modes.

- RAMAN Spectroscopy was studied for all the three compounds. Raman spectroscopy provides information about molecular vibrations that can be used for sample identification and quantization. The technique involves shining a monochromatic light source (i.e. laser) on a sample and detecting the scattered light. The majority of the scattered light is of the same frequency as the excitation source; this is known as Rayleigh or elastic scattering. A very small amount of the scattered light is shifted in energy from the laser frequency due to interactions between the incident electromagnetic waves and the vibrational energy levels of the molecules in the sample. Plotting the intensity of this "shifted" light versus frequency results in a Raman spectrum of the sample. The band positions will lie at frequencies that correspond to the energy levels of different functional group vibrations.

3.3 Flowchart of the steps:

INGREDIENTS TAKEN

↓ GRINDING FOR 3 HOURS

CALCINED AT 1000 DEGREE CENTIGRADE

↓ GRINDING FOR HALF AN HOUR

CALCINED AT 1100 DEGREE CENTIGRADE

↓ GRINDING FOR HALF AN HOUR

CALCINED AT 1200 DEGREE CENTIGRADE

↓ PELLETS FORMED APPLYING 2 TONS OF PRESSURE

SAMPLES CINTERED AT 1300 DEGREE CENTIGRADE

MEASUREMENTS MADE

XRD ANALYSIS   SEM IMAGES   FTIR   RAMAN

CHAPTER 4

Results & Discussions

4.1 X-Ray Diffraction Analysis:

Phase analysis is done using the room temperature powder X-Ray Diffraction (XRD) performed on a diffractometer **(PAN analytical X'Pert Pro)** using CuK_α (λ=1.5406 Angstrom) radiation at 30 kV and 40 mA. The scan rate used was 0.02^0/sec.

Using the intensity~2θ plots for all the three compounds, I have marked the prominent peaks along with their corresponding Miller Indices using JCPDS database. Using the θ value I have calculated the particle size and the strain from Debye-Scherrer technique.

Debye-Scherrer technique:

The significance of the broadening of peaks evidences grain refinement along with the large strain associated with the powder. The instrumental broadening (β_{hkl}) was corrected, corresponding to each diffraction peak of the material using the relation:

$\beta_{hkl} = [(\beta_{hkl})^2{}_{measured} - (\beta_{hkl})^2{}_{instrumental}]^{1/2}$

$\rightarrow$Average nanocrystalline size calculated using Debye-Scherrer's formula:

$D = \frac{K\lambda}{\beta hkl\ cos\theta}$, where D=crystalline size, K=Shape factor, λ=CuK_α wavelength.

$\rightarrow$Strain induced in powders due to crystal imperfection and distortion was calculated using the formula:

$\varepsilon = \frac{\beta hkl}{4\ tan\theta}$, where ε= strain induced.

Assuming that the particle size and strain contributions to line broadening are independent to each other and both have Cauchy like profile, the observed line breadth is

$\beta_{hkl} = \frac{K\lambda}{D\ cos\theta} + 4\varepsilon\ tan\theta$

implies, $\beta_{hkl}\ cos\ \theta = \frac{K\lambda}{D} + 4\varepsilon\ sin$This equation is known as W-H equation (from Williamson Hall technique)

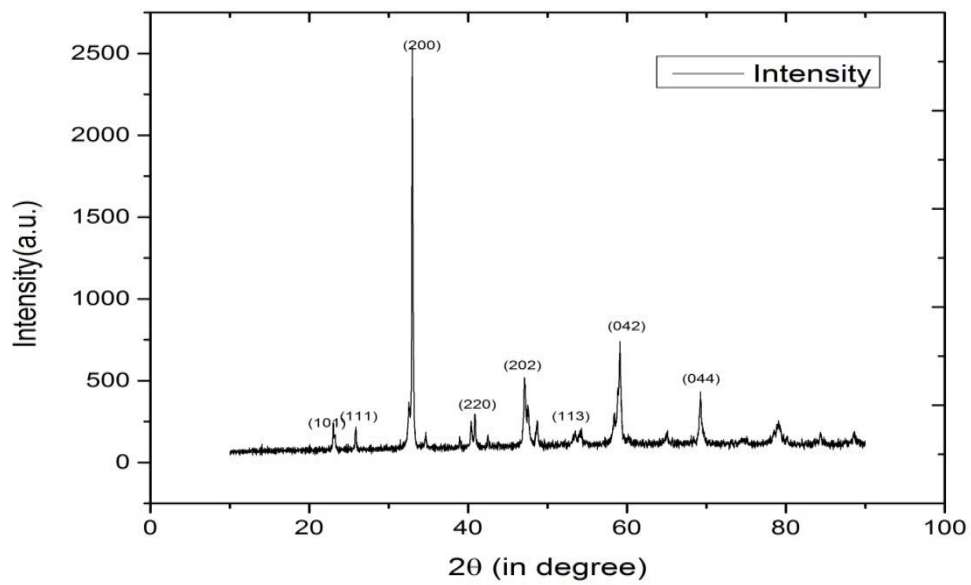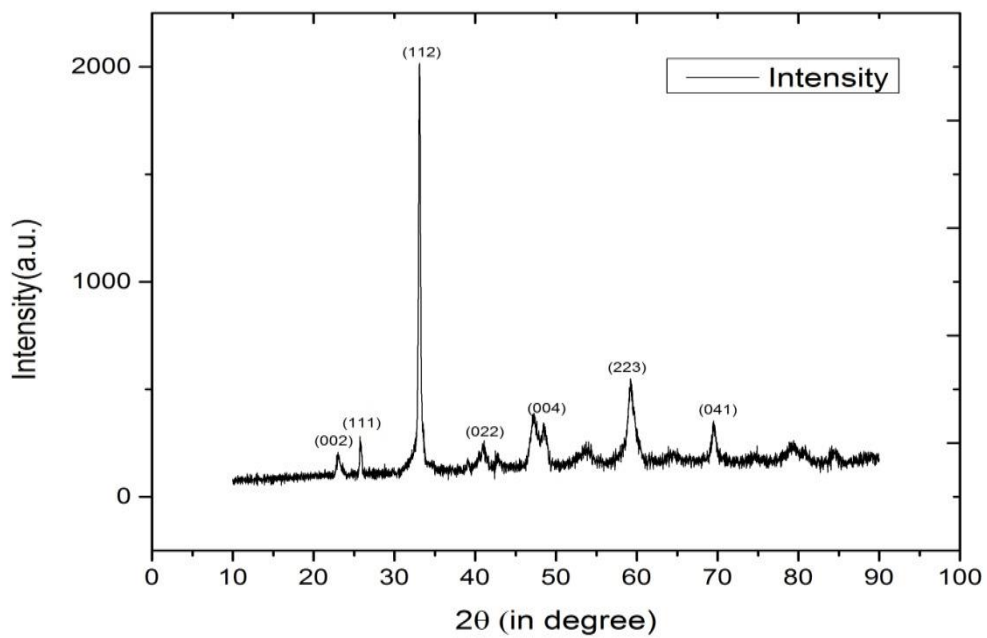**Fig 4.1** XRD pattern of $Gd_{0.7}Sr_{0.3}MnO_3$
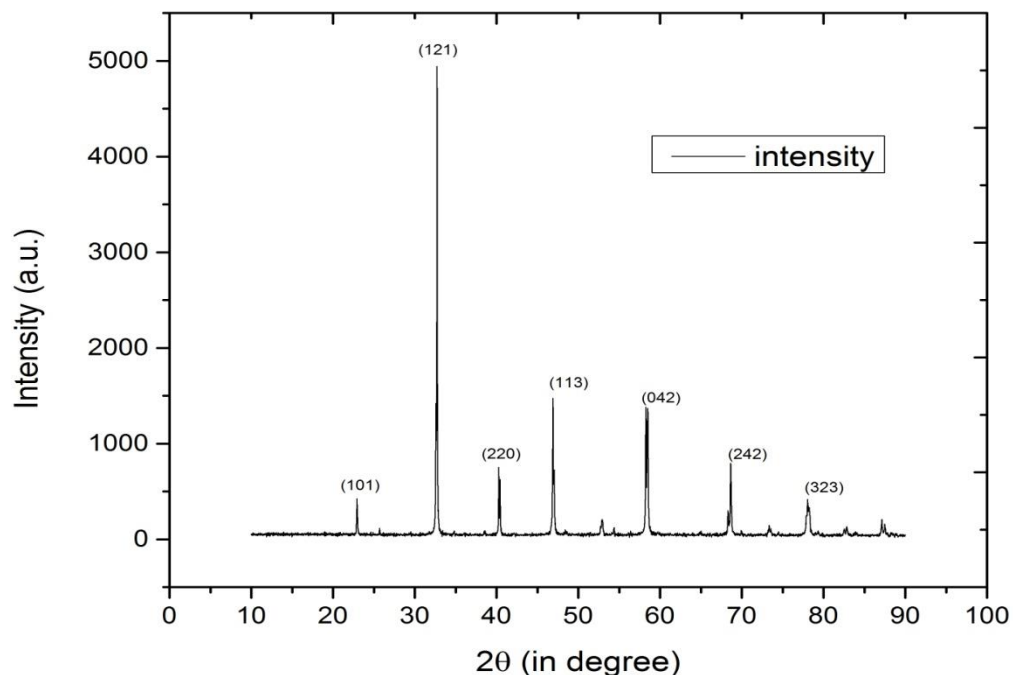

Fig-4.2 XRD pattern of $Pr_{0.7}Sr_{0.3}MnO_3$

Fig-4.3 XRD pattern of $Dy_{0.7}Sr_{0.3}MnO_3$

TABLE – 4.1 LATTICE PARAMETERS OF THE COMPOUND AND CALCULATION OF VOLUME FROM THE INTENSITY~2θ PLOTS

Compound name	a	b	c	V=abc
$Dy_{0.7}Sr_{0.3}MnO_3$	5.4777	7.7641	5.4664	232.483
$Gd_{0.7}Sr_{0.3}MnO_3$	5.4566	7.6409	5.4232	226.108
$Pr_{0.7}Sr_{0.3}MnO_3$	5.4563	7.6241	5.4056	224.868

[**NOTE** - a, b and c are lattice parameters in Å and V is Volume of the orthorhombic cell in $Å^3$]

The lattice parameters have been verified with JCPDS database and they are in well agreement with the JCPDS data value. [33]

TABLE – 4.2 CALCULATION OF PARTICLE SIZE AND STRAIN VALUES OF THE COMPOUNDS

$Gd_{0.7}Sr_{0.3}MnO_3$

2θ	sin θ	(hkl)	FWHM(rad)	β	β cos θ	tan θ	Particle size	strain
32.97	0.2838	(200)	0.0029	0.0028	0.0028	0.2960	501.73	0.0024
45.62	0.3876	(221)	0.0657	0.0657	0.0605	0.4206	22.90	0.0391
59.06	0.4928	(042)	0.0069	0.0069	0.0060	0.5665	230.18	0.0031
69.24	0.5681	(400)	0.0037	0.0036	0.0029	0.6905	470.39	0.0013
79.06	0.6364	(323)	0.0075	0.0075	0.0057	0.8254	241.25	0.0022
						Average →	293.29	0.0096

$Pr_{0.7}Sr_{0.3}MnO_3$

2θ	sin θ	(hkl)	FWHM(rad)	β	β cos θ	tan θ	Particle size	strain
25.83	0.2235	(111)	0.0066	0.0065	0.0064	0.2293	217.72	0.0071
33.11	0.2849	(020)	0.0049	0.0047	0.0045	0.2973	305.03	0.0039
47.33	0.4014	(220)	0.0183	0.0183	0.0167	0.4383	82.92	0.0104
59.30	0.4947	(132)	0.0152	0.0151	0.0132	0.5693	105.31	0.0067
69.53	0.5702	(040)	0.0105	0.0104	0.0086	0.6943	161.64	0.0038
						Average →	174.52	0.0064

$Dy_{0.7}Sr_{0.3}MnO_3$

2θ	sin θ	(hkl)	FWHM(rad)	β	β cos θ	tan θ	Particle size	Strain
22.94	0.1989	(101)	0.0021	0.0019	0.0018	0.2029	760.99	0.0023
32.72	0.2817	(121)	0.0017	0.0015	0.0014	0.2936	962.07	0.0013
40.34	0.3448	(220)	0.0046	0.0045	0.0042	0.3674	329.65	0.0031
46.93	0.3982	(202)	0.0039	0.0039	0.0035	0.4341	394.24	0.0023
50.41	0.4258	(230)	0.0067	0.0066	0.0059	0.4706	231.75	0.0035
						Average →	535.76	0.0025

NOTE ---

PARTICLE SIZE IS IN ANGSTROM (1 ANGSTROM = 10^{-10}m)

STRAIN IS DIMENSIONLESS

The particle size and the strain values have been verified with other published resources of LSMO that belongs to the class of the compounds that I have studied, and has well agreed [32].

4.2 SEM Image Analysis:

The SEM images reveal that the grain boundaries are not clear and there is poor homogeneity and much porosity in all the samples.

The SEM images have been shown below for all the three compounds along with the grain size distribution curve for $Dy_{0.7}Sr_{0.3}MnO_3$ and $Gd_{0.7}Sr_{0.3}MnO_3$.
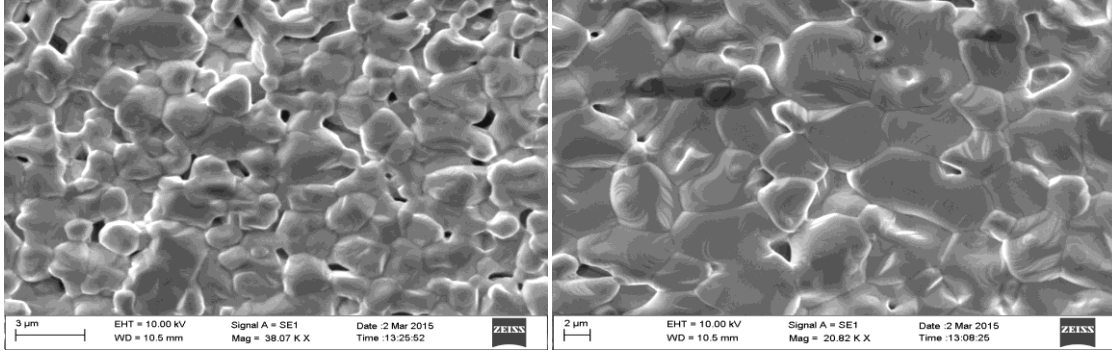
Fig-4.4 SEM Image for $Gd_{0.7}Sr_{0.3}MnO_3$ **Fig-4.5** SEM Image for $Dy_{0.7}Sr_{0.3}MnO_3$

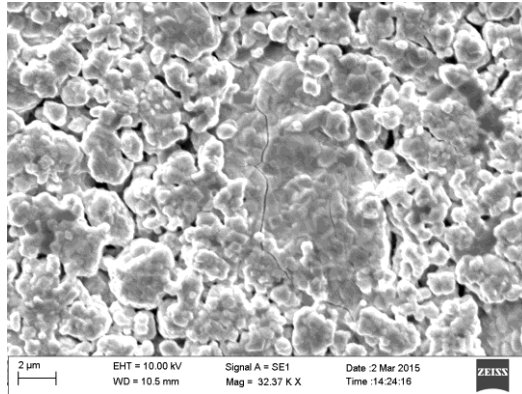**Fig-4.6** SEM Image for $Pr_{0.7}Sr_{0.3}MnO_3$

The SEM images were taken using **SEM-Zeiss EVO 18 Special Edition**.

The mean grain size for the $Dy_{0.7}Sr_{0.3}MnO_3$ compound comes out to be 4.785 μm and for $Gd_{0.7}Sr_{0.3}MnO_3$ it comes out to be 1.817 μm. [33]

The $Pr_{0.7}Sr_{0.3}MnO_3$ sample is too uneven to measure the grain size and draw the grain distribution curve. Thus the mean grain size for this sample has not been found out.
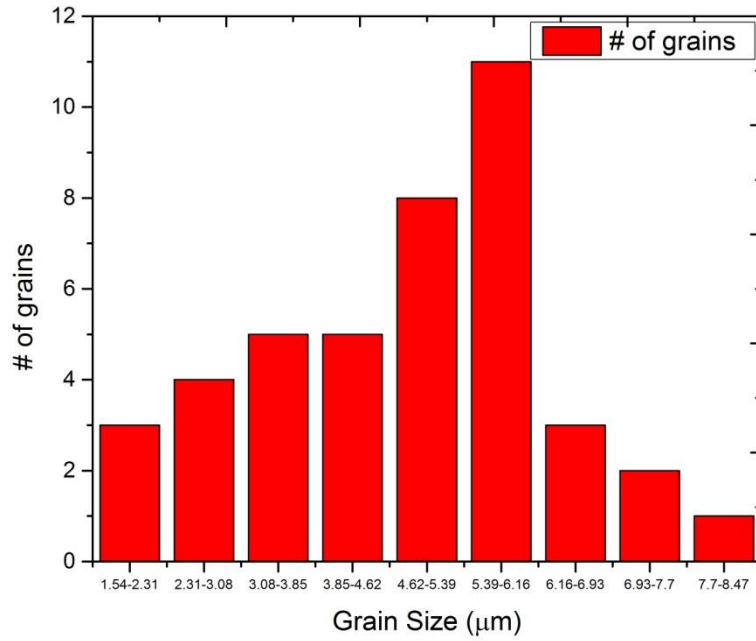
Fig-4.7 Grain size distribution of $Dy_{0.7}Sr_{0.3}MnO_3$

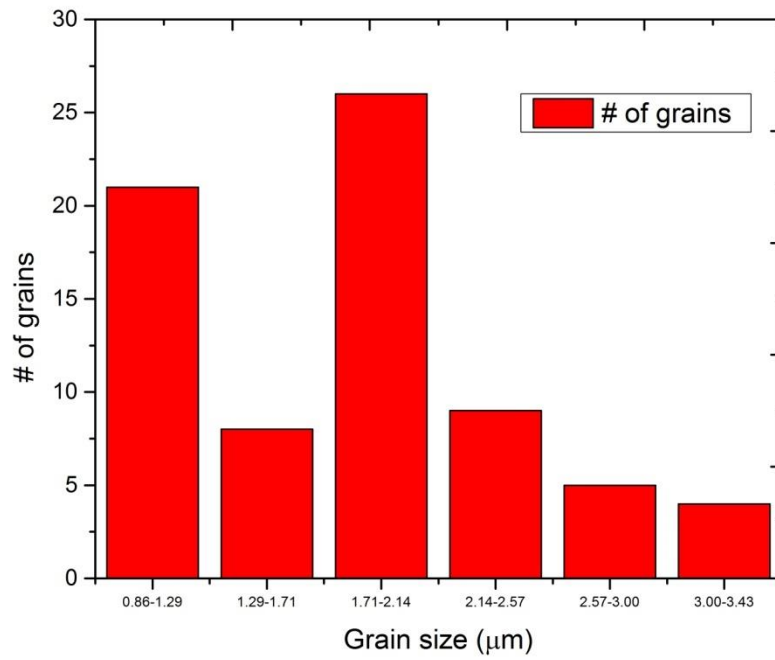**Fig-4.8** Grain size distribution of $Gd_{0.7}Sr_{0.3}MnO_3$

4.3 FTIR Analysis (Fourier Transform Infrared Spectroscopy):

IR spectroscopy deals with the interaction between a molecule and radiation from the IR region of the electromagnetic spectrum ($4000cm^{-1}$ to $400cm^{-1}$). The cm^{-1} unit is the wave number scale and is given by 1/wavelength.

IR radiation causes the excitation of the vibrations of covalent bonds within that molecule. These vibrations include the stretching and bending modes. An IR spectrum show the energy absorptions as one 'scans' the IR region of the EM spectrum. In general terms it is convenient to split an IR spectrum into two approximate regions:

4000-1000 cm^{-1} (known as the functional group region)

<1000 cm^{-1} (known as the fingerprint region)

Since from physics point of view we are only interested in the modes of vibration, it is enough for us to analyze the spectrum in the fingerprint region.

The FTIR analysis has been done using **Bruker ALPHA FT-IR**.

Analysis of the FTIR spectrums show sharp peaks at

555.2 and 588.4 cm^{-1} for the compound $Pr_{0.7}Sr_{0.3}MnO_3$

548.2 and 584.9 cm^{-1} for the compound $Gd_{0.7}Sr_{0.3}MnO_3$

556.8 and 578.8 cm^{-1} for the compound $Dy_{0.7}Sr_{0.3}MnO_3$

The FTIR spectra for this family of compounds show two absorption peaks in and around 530 cm^{-1} to 590 cm^{-1} .[26] These bands that are located nearer to 600 cm^{-1} are attributed to the combination of stretching mode of Mn-O-Mn and bending mode of Mn-O bonds. These two bands are related to the environment surrounding the MnO_6 octahedra and the local modes of the MnO_6 octahedra. The peaks are sensitive to the octahedral distortion and the lowering of symmetry arising due to Jahn Teller effect.[27] [31]
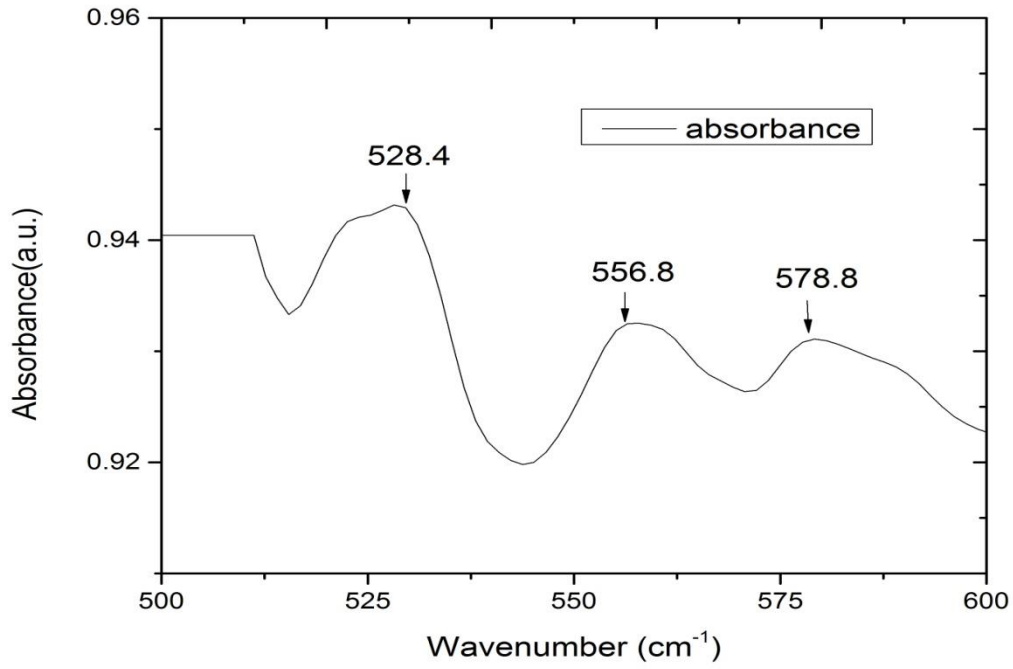
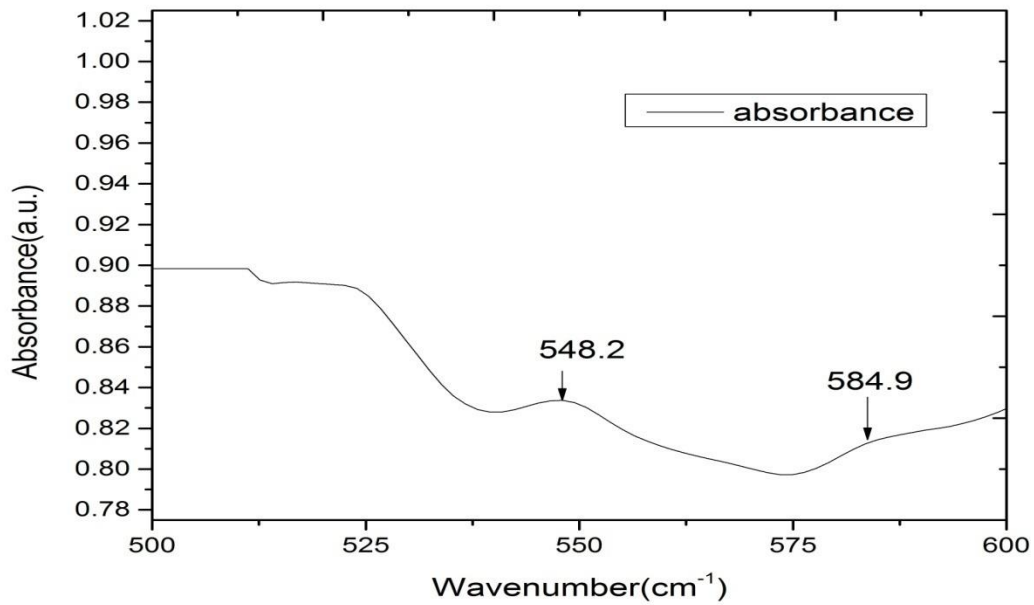**Fig-4.9** FTIR spectrum for $Dy_{0.7}Sr_{0.3}MnO_3$

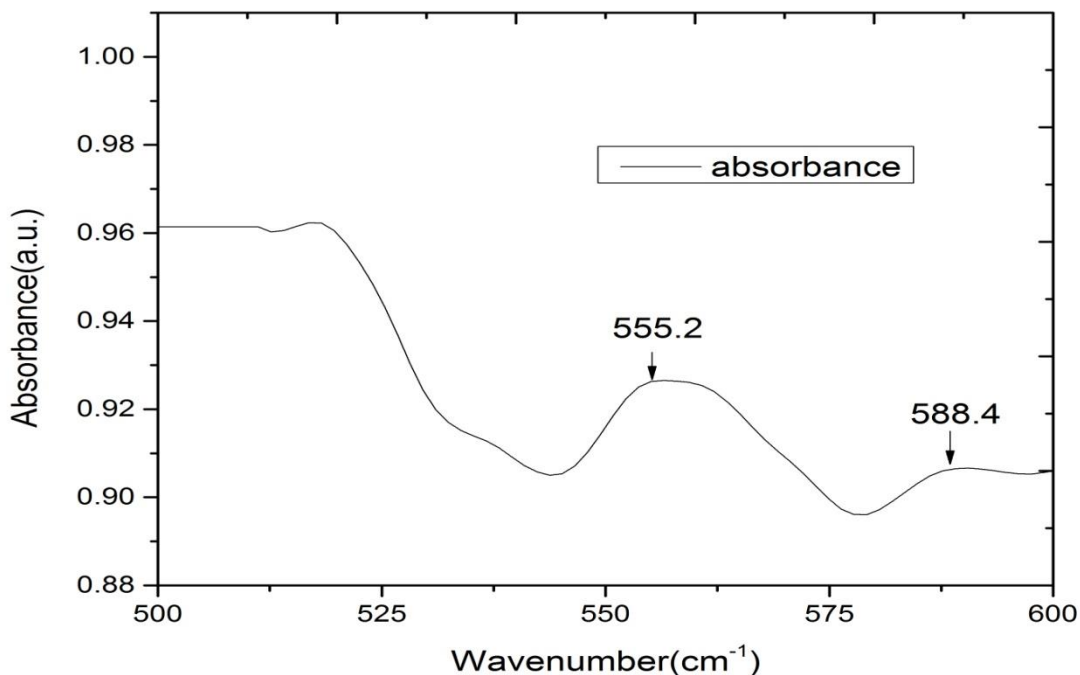**Fig-4.10** FTIR spectrum for $Gd_{0.7}Sr_{0.3}MnO_3$

Fig-4.11 FTIR spectrum for $Pr_{0.7}Sr_{0.3}MnO_3$

4.4 RAMAN Spectra Analysis:

Raman spectroscopy is complementary to IR spectroscopy and in this case a net change in bond polarizability must be observed for a transition to be Raman active.

Model described in terms of a minimum set of fundamental vibrations, based on a threefold set of co ordinate axes (known as normal mode of vibration)

Number of normal modes = 3N-6 (Nonlinear)

= 3N-5 (Linear), where N is number of component atoms in the molecule.

Raman analysis has been done for all the three compounds and the peaks have been marked. The peaks have been identified and correlated with specific vibrational modes.

The Raman Spectroscopy was performed using a **source wavelength of 785 nm, 10mW power source** and 20 seconds of detecting time. The spot was a 50 μm circular spot.

From the figures given below we can find prominent peaks for all the 3 compounds. They are as follows:

$Dy_{0.7}Sr_{0.3}MnO_3$ → 217.1, 310.7, 480.7 and 627.3 cm^{-1}

$Gd_{0.7}Sr_{0.3}MnO_3$ → 229.6, 337.8, 468.2 and 608.9 cm^{-1}

The peaks of $Pr_{0.7}Sr_{0.3}MnO_3$ sample could not be analyzed properly since the peaks are not prominent and sharp as we can see from the plot given below. This could be due to noise formation while taking the data.

Now as we can see the peaks at four specific ranges. The lines of a certain range have their own modes of vibration.

200-250 cm^{-1} correspond to the out of phase rotation of the oxygen cage i.e. apical oxygen bending or rotation of the octahedral.

310-340 cm^{-1} mode correspond to the Mn-O bond stretching.

460-480 cm^{-1} correspond to the bending mode of the MnO_6 octahedra.

600-630 cm^{-1} correspond to the in phase stretching and Jahn Teller distortion. [29] [30]
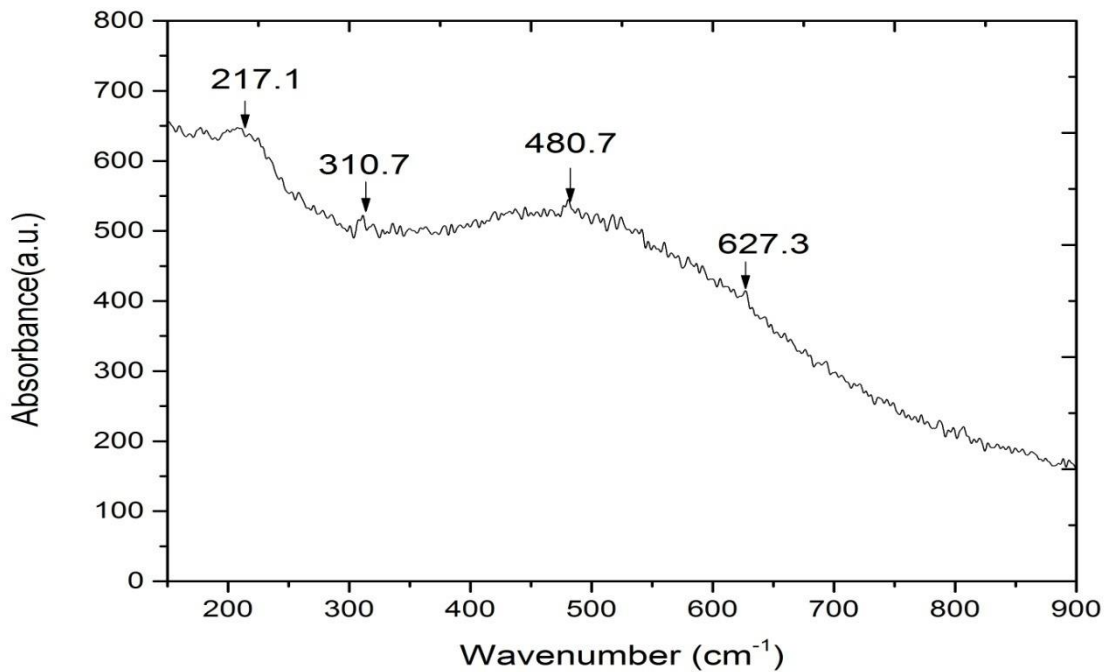

Fig-4.12 Raman spectrum for $Dy_{0.7}Sr_{0.3}MnO_3$
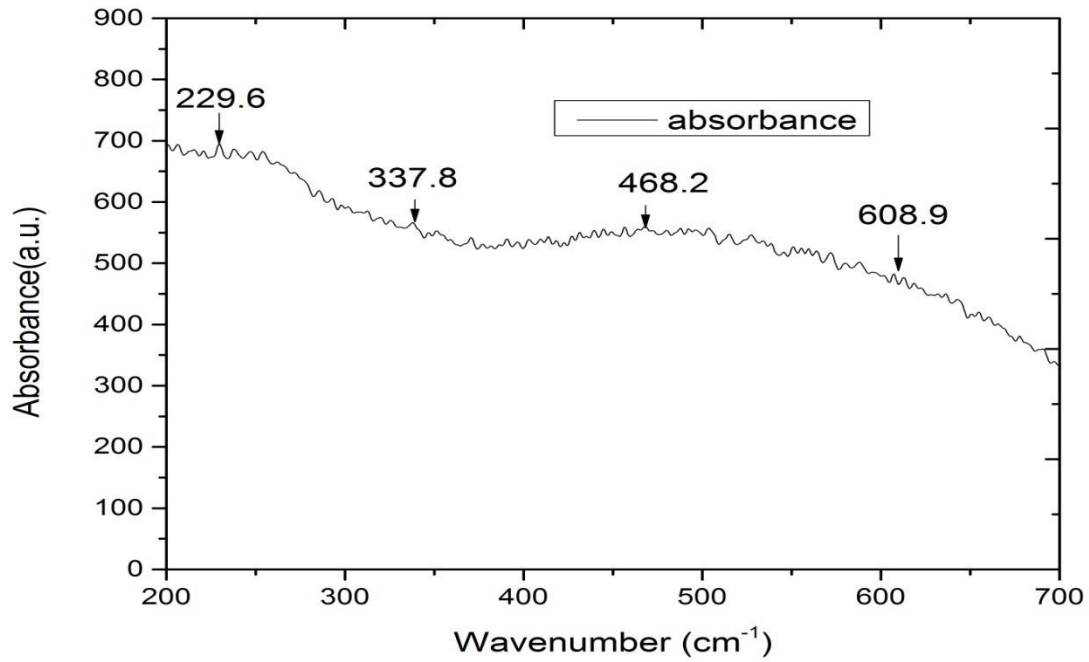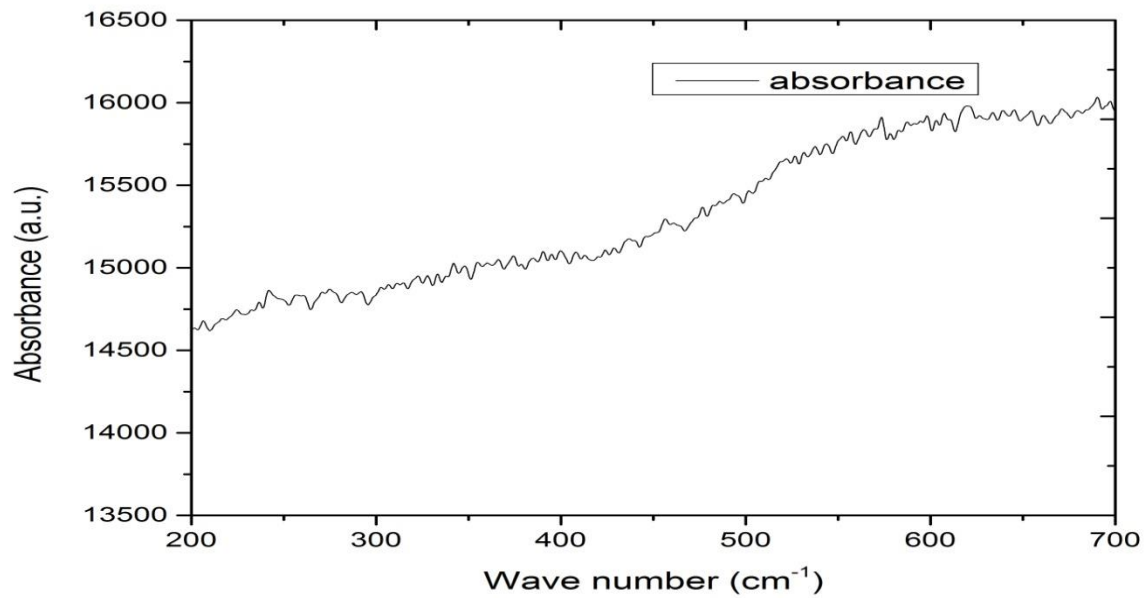
Fig-4.13 Raman spectrum for $Gd_{0.7}Sr_{0.3}MnO_3$

Fig-4.14 Raman spectrum for $Pr_{0.7}Sr_{0.3}MnO_3$

Chapter 5

Conclusion & Future directions:

The samples of $Pr_{0.7}Sr_{0.3}MnO_3$, $Gd_{0.7}Sr_{0.3}MnO_3$ and $Dy_{0.7}Sr_{0.3}MnO_3$ have been prepared successfully by solid state synthesis route. The x-ray diffraction shows sharp and well defined peaks for the compounds. On comparing the x-ray diffraction results to JCPDS database the structure of the compounds is found to be orthorhombic and their lattice parameters have well matched too with the JCPDS database. Further from the XRD readings the particle size and strain value has also been calculated using Debye Scherrer technique. The average particle size has come out to be 29.3nm, 17.4nm and 53.5nm for $Gd_{0.7}Sr_{0.3}MnO_3$, $Pr_{0.7}Sr_{0.3}MnO_3$ and $Dy_{0.7}Sr_{0.3}MnO_3$ respectively.

Next the SEM images have also been taken which show that the grain boundaries are not clear and there is poor homogeneity and much porosity in all the samples. The grain size distribution curve has been plotted and the nature of the curve has come out to be Gaussian. The mean grain size for the $Dy_{0.7}Sr_{0.3}MnO_3$ compound comes out to be 4.785 μm and for $Gd_{0.7}Sr_{0.3}MnO_3$ it comes out to be 1.817 μm.

The FTIR curve has also been plotted in the range 400-1000 cm^{-1} and the peak values have been noted in the absorbance versus wave number plot. The peaks denote the values at which the octahedral distortion takes place and the lowering of symmetry due to the Jahn Teller effect. The peak values have been obtained in the wave number region of 500-600 cm^{-1}.

Raman spectroscopy has also been performed to complement the FTIR analysis. The peak values for the Raman spectra again confirm the orthorhombic symmetry of the compounds as observed from XRD analysis. We also found out the vibrational modes from the Raman Spectra and the regions of distortion of MnO_6 octahedra and Jahn Teller distortion.

The work can be further extended to analyze the transport properties of the compounds and to find out the Temperature ~ Resistivity curves. This curve can give us an idea of the temperature at which the metal insulator transition takes place. The temperature coefficient of resistance can be further found out and drop in resistivity can be utilized for bolometric applications. Ferromagnetic to paramagnetic transition temperature can also be found out as well thus determining the Curie temperature.

REFERENCES

[1] M.C. Brant, L. Dessemond, Solid State Ionics 138 (2000) 1–17.

[2] D. Stover, H.P. Buchkremer, S. Uhlenbruck, Ceram. Int. 30 (2004) 1107–1113.

[3] D.Z.D. Florio, F.C. Fonseca, E.N.S. Muccillo, R. Muccillo, Ceramica 50 (2004) 275–290.

[4] S.J. Stephen, Int. J. Inorg. Mater. 3 (2001) 113–121.

[5] T. Horita, K. Yamaji, N. Sakai, Y. Xiong, T. Kato, H. Yokokawa, T. Kawada, J. Power Sources 106 (2002) 224–230.

[6] E.P. Murray, T. Tsai, S.A. Barnett, Solid State Ionics 110 (1998) 235–243.

[7] A. Barbucci, R. Bozzo, G. Cerisola, P. Costamagna, Electrochim. Acta 47 (2002) 2183–2188.

[8] A. Barbucci, P. Carpanese, G. Cerisola, M. Viviani, Solid State Ionics 176 (2005) 1753–1758.

[9] A. Barbucci, M. Viviani, P. Carpanese, D. Vladikova, Z. Stoynov, Electrochim. Acta 51 (2006) 1641–1650.

[10] J. Deseure, Y. Bultel, L. Dessemond, E. Siebert, Electrochim. Acta 50 (2005) 2037–2046.

[11] V.V. Srdi´ c, R.P. Omorjan, J. Seydel, Mater. Sci. Eng. B 116 (2005) 119–124.

[12] X. Deng, A. Petric, J. Power Sources 140 (2005) 297–303.

[13] H.Y. Jung, W.S. Kim, S.H. Choi, H.C. Kim, J. Kim, H.W. Lee, J.H. Lee, J. Power Sources 155 (2006) 145–151.

[14] X.J. Chen, K.A. Khor, S.H. Chan, J. Power Sources 123 (2003) 17–25.

[15] M. Kuznecov, P. Otschik, P. Obenaus, K. Eichler, W. Schaffrath, Solid State Ionics 157 (2003) 371–378.

[16] Y. N. Lee, Perovskitas sustituidas $Ln_{1-x}A_x MnO_3$ (Ln = La, Nd; A = K, Sr): sintesis por vias no convencionales, propiedades cataliticas y de magnetotransporte, PhD thesis, Universidad de Valencia, Valencia, 1997.

[17] F.W. Poulsen, Solid State Ionics 129 (2000) 145–162.

[18] P. Ciambelli, S. Cimino, L. Lisi, M. Faticanti, G. Minelli, I. Pettiti, P. Porta, Appl. Catal. B 33 (2001) 193–203.

[19] J.H. Kuo, H.U. Anderson, D.M. Sparlin, J. Solid State Chem. 87 (1990) 55–63

[20]Ramirez, A. P.J. Phys: Condens. Matter1997,9, 8171.

[21] Rao, C. N. R., Raveau, B., Eds. Colossal magnetoresistance and other related properties in 3d oxides; World Scientific: Singapore, 1998

[22] De Silva, P. S. I. P. N.; Richards, F. M.; Cohen, L. F.; Alonso, J. A.;Martınez-Lope, M. J.; Casais, M. T.; Thomas, K. A.; MacManus-Driscoll, J. L.J. Appl. Phys.1998,83, 394.

[23] Ghivelder, L.; Abrego-Castillo, I.; Gusmão, M. A.; Alonso, J.A; Cohen,L. F.Phys. ReV.B 1999,60, 12184

[24] M. N. Iliev, M. V. Abrashev,V. N. Popov,V. G. Hadjiev , PHYSICAL REVIEW B 67, 212301 ~2003

[25] I. A. Abdel-Latif, JOURNAL OF PHYSICS VOL. 1 NO. 3 Oct. (2012) PP. 15-31

[26] P. T. Phong , S. J. Jang , B. T. Huy ,Y.-I. Lee ,I.-J. Lee, J Mater Sci: Mater Electron (2013) 24:2292–2301 DOI 10.1007/s10854-013-1092-7

[27] Abir Nasri , S. Zouari , M. Ellouze , J.L. Rehspringer, A.-F. Lehlooh ,F. Elhalouani , J Supercond Nov Magn (2014) 27:443–451 DOI 10.1007/s10948-013-2282-5

[28] Raman Scattering in Materials Science, By Willes H. Weber, Roberto Merlin

[29] A E Pantoja, H J Trodahl, R G Buckley, Y Tomioka ,Y Tokura J. Phys.: Condens. Matter 13 (2001) 3741–3752

[30] Scanning Raman spectroscopy for characterizing compositionally spread films Venimadhav. A, Yates K. A., Blamire M. G.

[31] Maneesha Gupta, Poonam Yadav, Wasi Khan, Ameer Azam, Alim H. Naqvi, R.K. Kotnala, Adv. Mat. Lett. 2012,3(3), 220-225

[32] http://shodhganga.inflibnet.ac.in/bitstream/10603/707/17/17.%20chapter5.pdf

[33] Guilherme Oliveira Siqueira, Rose Marie Belardi, Pedro Hespanha Almeida, Charles Luis da Silva, Marcia Caldeira Brant, Tulio Matencio, Rosana Zacarias Domingues, Journal of Alloys and Compounds 521 (2012) 50– 54

WEBSITE: (for some additional information)

http://abulafia.mt.ic.ac.uk/shannon/ptable.php